Numerical simulation of plasma discharge in RF ion thruster

IEPC-2019-496

Presented at the 36th International Electric Propulsion Conference
University of Vienna • Vienna, Austria
September 15-20, 2019

R.G. Rakhimov[1],Ya.Yu.Kharlan.[2] and I. Uzhinsky[3]
Skolkovo Institute of Science and Technology, Skolkovo Innovation Center, Nobel str. 3, Moscow, 121205, Russia

A.E. Milov [4] , R.E. Aypov[5] and I.A.Cherniy[6]
Avant – Space Systems LLC, Skolkovo Innovation Center, Nobel str. 7-20, Moscow, 121205, Russia

Abstract: The article presents a scheme for the complex calculation of the parameters of a radio-frequency ion thruster. The share of power losses due to spurious induction heating of metal elements of the thruster, the discharge plasma parameters; heat fluxes and temperature fields and thruster operating modes. In the course of experimental work, using indirect measurements and measurements by Faraday probes, the ion current values were determined. Comparison of calculation results and experimental data is analyzed. The corresponding recommendations for the design of engines of this type are proposed.

Nomenclature

q_e	=	elementary charge
k_B	=	Boltzmann constant
m, M	=	electron and atom mass
V	=	discharge chamber volume
A	=	total discharge chamber area
l	=	discharge chamber length
R	=	discharge chamber radius
A_w	=	discharge chamber wall area
A_s	=	total screen grid area
f_s, f_a	=	transparency for ions (screen grid transparency) and for neutrals (accel grid transparency)
Q	=	neutrals flow rate (s-1)
K_{ex}	=	rate coefficients for electron-impact excitation
K_{iz}	=	rate coefficients for electron-impact ionization
K_{el}	=	rate coefficients for electron-impact elastic scattering
K_{in}	=	the rate for ion-neutral elastic collisions
κ	=	xenon gas thermal conductivity
Λ_0	=	heat diffusion length
U_{iz}	=	potential of ionization
U_{ex}	=	average potential of excitation
υ_g	=	mean velocity of atoms

[1] PhD student, Center for Design and Materials, ruslan.rakhimov2@skoltech.ru.
[2] PhD student, Center for Design and Materials, iana.kharlan@skoltech.ru.
[3] Full Professor, Head of Center for Design and Materials, i.uzhinsky@skoltech.ru
[4] PhD, Structural Engineer, a.milov@avantspace.com
[5] System Engineer, rodion.ayupov@avantspace.com
[6] Design engineer, cherniy@avantspace.com

I. Introduction

THE number of small satellites launched annually is experiencing rapid growth, and this is often attributed to the current trend of creating small satellite constellations in low orbits. The biggest space companies such as OneWeb and SpaceX have announced their intention to launch of thousands of satellites in the next 5 years [1, 2]. This fact puts forward serious requirements for the spacecraft production, such as the relatively low cost and spacecraft creation time and the increase in the duration of active existence. The creation of groupings from a large number of spacecraft requires the ability to carry out a spacecraft dilution along the orbit. Moreover, the concept of formation (or swarm) of satellites also implies increased costs of the working fluid to maintain the orbital construction of such a grouping. This leads to the need for a small propulsion system with a high specific impulse [3].

In this regard, the main goal of the Avant Space Systems start-up project is creation a compact efficient propulsion system based on a radio frequency (RF) inductively coupled discharge in an external magnetic field [4]. At this stage, the company has developed bench-mounted power sources (RF generator and high voltage power supply) and a thruster laboratory model. The purpose of which is to study ongoing processes and study factors that affect the efficiency and performance of the engine. In the design process of the propulsion system, a complex approach was taken to simulate the thruster physical processes. During the study, the calculated process models and the complex simulation scheme are constantly updated and verified according to the obtained experimental data. The steps of calculating and developing the lab model are described in this article. Chapter II describes a complex approach to calculating the classical design of an RF ion thruster, including the calculation of plasma parameters and heat fluxes, simulation the processes of an ion-optical system (IOS), determining the fraction of power losses due to induction heating and calculating the temperature conditions of the thruster. Chapters III and IV describe the current configuration of the laboratory engine model, the used vacuum facility and the engine performance diagnostic systems. Also in these chapters is a comparison of the experimentally measured beam current with the calculated results for different operating modes. Chapter V presents the current research conclusion and plans for the future.

II. Complex calculation

The development of an RF ion thruster requires a deep understanding of the physics of processes in a radio-frequency inductively coupled discharge. As a result of the large number of interconnected processes occurring in the engine nodes, it is incorrect to consider them separately. For example, as a result of induction losses in the structural details and skin effect in the conductive elements, the useful power of the generator can be lost up to tens of percent. In the process of plasma interaction with surrounding parts, temperature heating and thermal deformation of engine elements occur, and the temperature-dependent properties of materials change. Thermal deformations of the IOS have a significant effect on the ion beam focusing, and, consequently, on the traction and operational life characteristics of the propulsion system. All these factors, to varying degrees, affect the engine operating modes and its characteristics. Therefore, the discrepancy between the calculated data and the experimental results can be associated not only with the errors of the plasma model, but also with the influence of related factors. Consideration of all these factors in the framework of a single plasma model is currently impossible. In order to increase the accuracy of the calculation, a complex scheme of calculating and optimizing the structural and traction characteristics of the engine was implemented. Based on the proposed scheme, a laboratory model of the engine was designed to study the influence of parameters on the characteristics of the thruster, including the influence of an external magnetic field. The optimization cycle for calculating the RF ion thruster is shown in Figure 1.

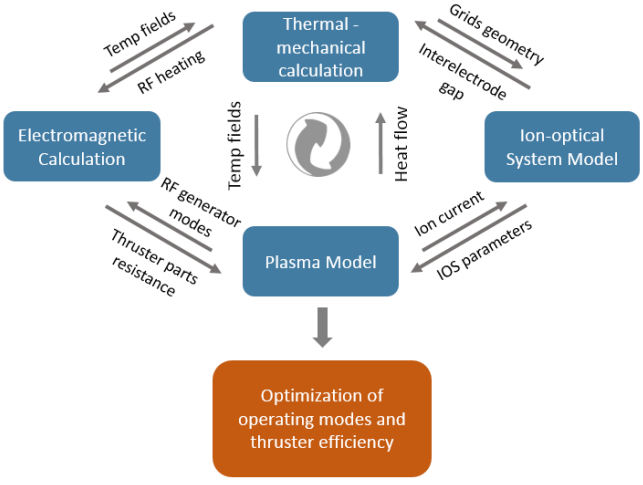

Figure 1. The complex calculation scheme of the RF ion thruster

At the first stage of the cycle, the geometric parameters of the electrodes and the ion-optical system (IOS) potentials are determined. Next, the share of losses of the input RF power for induction heating of the thruster metal elements

for the selected operating mode is calculated. The characteristics of the discharge plasma and heat fluxes to the surrounding parts are found. Using the obtained data, a thermomechanical calculation of the engine is performed.

At the second stage, the input data is refined. Using the information obtained on the electrodes temperature deformations, the minimum possible grid gap is found. The hole diameters and IOS potentials are specified by the deviation of the holes from the alignment as a result of thermal displacement and technological production capabilities. Using the new IOS parameters, the electromagnetic properties and plasma and beam parameters are recalculated, and new temperature conditions are determined. The cycle was repeated until an acceptable operating mode and engine configuration were found. The controlled parameters were the beam current and the thermal state of the engine. In the end, according to the data obtained, the traction characteristics of the thruster and its efficiency were evaluated.

A. Ion-optical system parameters

The ion-optical system of the thruster is a unit that determines both the efficiency of ion extraction and the engine operational life. In the calculation, for the selected beam diameter, the diameters of the holes, their number and location were selected with the condition of obtaining the maximum ion transparency of the electrodes.

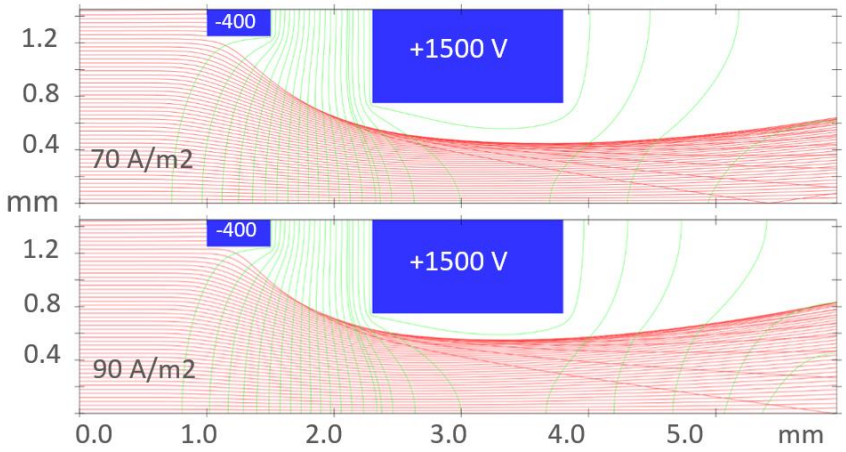

Figure 2. The results of ion beam motion simulation in the ion-optic system

Using the open source IBSIMU program code [5], the motion of the ion beam in one of the IOS apertures was simulated (Figure 2). According to the calculation results, the most suitable electrode thicknesses and interelectrode gaps were found. Using preliminary ranges of ion current densities and engine operating modes, the necessary potentials on the grids were determined. According to the results of chapter II.F, the selected interelectrode gap was adjusted based on the thermal deformation of the electrodes during thruster operation.

B. Radio-frequency power losses

The radio-frequency fields create eddy currents in metal elements, which act as an additional source of heating and reduce the fraction of the useful power absorbed in the plasma. The magnitude of the power loss strongly depends on the design features of the product, such as the material of the parts and the proximity of their location to the inductor. In order to determine the share of power losses, the calculation was performed in the COMSOL Multiphysics software package (Magnetic and electric fields module). After a series of calculations for the selected thruster configuration, it was revealed that the inductance and resistance of the inductor do not depend on the current amplitude, but depend only on its frequency and the presence of surrounding metal parts. As a result of the simulation, the dependences of the

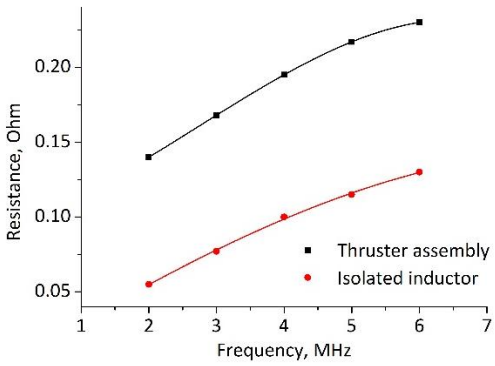

Figure 3. Dependences of the active resistances of an isolated inductor and thruster assembly on the current frequency

resistance of the isolated inductor and the thruster assembly as a whole on the RF generator frequency were determined (Fig. 3).

Since the resistance of metals depends on temperature, at the stage of refinement, the resistance of the inductor and parts was recalculated according to the empirical formula:

$$R_T = R_0(1 + \alpha \cdot \Delta T), \qquad (1)$$

where α is the temperature coefficient of resistance (1/°C), ΔT is the difference between the current object temperature and room temperature.

C. Plasma parameters calculation

The discharge parameters were simulated using a hydrodynamic plasma model based on papers by P. Chabert [6] and D. Goebel [7]. The main dependences of the model were the equations of energy and particle balance, where the independent variables are the density and temperature of the neutrals (n_g, T_g) and electrons (n, T_e).

Particle balance equations:

$$\frac{dn}{dt} = nn_g K_{iz} - \frac{(I_{se} + I_{we})}{V q_e}, \qquad (2)$$

$$\frac{dn_g}{dt} = \frac{Q}{V} + \frac{(I_{si} + I_{wi})}{V q_e} - nn_g K_{iz} - \frac{n_g \upsilon_g A_g}{4V} \qquad (3)$$

Energy balance equations:

$$\frac{d}{dt}\left(\frac{3}{2} n_g k_B T_g\right) = 3\frac{m}{M} k_B (T_e - T_g) n n_g K_{el} + \frac{1}{4} M \upsilon_B^2 n n_g K_{in} - \kappa \left(\frac{T_g - T_w}{\Lambda_0}\right)\frac{A}{V} \qquad (4)$$

$$\frac{d}{dt}\left(\frac{3}{2} n k_B T_e\right) = W_{abs} - W_{loss}, \qquad (5)$$

where υ_B is the Bohm velocity, T_w is the temperature of the discharge chamber walls.

The dependences of the averaged cross sections for the interaction of various kinds of particles (K_{iz}, K_{el}, K_{in}) were taken from the D. Goebel's textbook [8].

In considering the quasi-neutral plasma volume, the currents of ions and electrons to the dielectric walls of the discharge chamber and electrodes are determined by the following relationships:

$$I_{we} = \frac{n}{4} q_e \sqrt{\frac{8 k_B T_e}{\pi m}} A_w \, exp\left\{-\frac{q_e \phi_w}{k_B T_e}\right\}, \qquad (6)$$

$$I_{wi} = 0.6\, n q_e \sqrt{\frac{k_B T_e}{M}} A_w, \qquad (7)$$

$$I_{se} = \frac{n}{4} q_e \sqrt{\frac{8 k_B T_e}{\pi m}} (1 - f_s) A_s \, exp\left\{-\frac{q_e \phi_s}{k_B T_e}\right\}, \qquad (8)$$

$$I_{si} = 0.6\, n q_e \sqrt{\frac{k_B T_e}{M}} (1 - f_s) A_s, \qquad (9)$$

$$I_b = 0.6\, n q_e \sqrt{\frac{k_B T_e}{M}} f_s A_s, \qquad (10)$$

where f_s is the transparency of the emission electrode for ions, calculated in Chapter II.A.

According to the theory of sheath-layer [9], in the presence of dielectric or metal walls under a floating potential, the conditions for particles to leave on the wall must satisfy the condition of equality of the density of electron and ion currents. Since the mobility and thermal velocity of electrons far exceeds the mobility of ions, a sheath layer should be established near the surface in which the condition of quasi-neutrality is violated and a potential barrier for electrons is established between the wall and the unperturbed plasma. The sheath layer creates a potential barrier for electrons, due to which its fastest component is retained in the plasma. The height of the barrier is maintained in such a way that the condition of current continuity is fulfilled, i.e., a balance is maintained between the generation and loss of charged particles in the plasma. In particular, if the wall is insulated, then the fluxes of ions and electrons to this wall should be equal.

$$I_{we} = I_{wi}, \qquad (11)$$

$$\phi_w = \frac{k_B T_e}{q_e} ln\left\{\frac{5}{6}\sqrt{\frac{2M}{\pi m}}\right\}, \qquad (12)$$

The potential drop near the surface of the screen grid is less due to the partial departure of the ion flux from the plasma into the electrode holes:

$$I_{se} = I_{si} + I_b, \qquad (13)$$

$$\phi_s = \frac{k_B T_e}{q_e} ln\left\{(1-f_s)\frac{5}{6}\sqrt{\frac{2M}{\pi m}}\right\}, \qquad (14)$$

The absorbed volumetric power was determined by the transformer model proposed by P. Chabert in articles [6, 10] as a function of the equivalent plasma resistance R_{ind} and the amplitude value of the current I_{coil} in the inductor.

$$W_{abs} = \frac{1}{2V} R_{ind} I_{coil}^2, \qquad (15)$$

Total losses of input volumetric power include energy losses due to ionization, excitation of neutral atoms, heating of a neutral gas as a result of elastic interaction, and losses due to the escape of electrons on the discharge chamber surface:

$$W_{loss} = U_{iz} q_e n n_g K_{iz} + U_{ex} q_e n n_g K_{ex} + 3\frac{m}{M} k_B (T_e - T_g) n n_g K_{el} + \frac{1}{V}[I_{es}(2T_e + \phi_s) + I_{ew}(2T_e + \phi_w)], \qquad (16)$$

The total power transmitted by the RF generator is determined by the equivalent plasma resistance and the total resistance of the surrounding parts and inductor R_{str}, calculated in Chapter II.B:

$$P_{RF} = P_{abs} + P_{str} = \frac{1}{2}(R_{ind} + R_{str}) I_{coil}^2, \qquad (17)$$

A system of four first-order nonlinear differential equations *(1)* - *(4)* was calculated by numerical integration by the Runge-Kutta (SciPy python library dop853) method until a stationary state was established. Stationary values of the calculated values were used to calculate subsequent thruster characteristics.

This model considers the dependences only for neutrals and electrons, the ions temperature is assumed to be equal to a neutral gas temperature, and the number density of ions is equal to electrons. The obtained plasma parameters are averaged over the volume, the electron velocity distribution function is considered Maxwellian, the ionization process is considered a one-step process, and the contribution of secondary ions is not taken into account. All these approximations limit the scope of this model and can cause deviation with experimental data.

D. Heat flow

Using the results of the calculation of the plasma parameters from Chapter II.C, the heat fluxes to the plasma surrounding thruster elements were calculated [11, 12].

The total power balance of the discharge can be written as:

$$P_{abs} = P_{scat} + P_w + P_{se} + P_{si} + P_{xw} + P_{xs} + P_{xa} + P_{xout} + P_b, \qquad (18)$$

where Pscat is the power lost during elastic scattering of electrons by a neutral particle; Pw — heating of the discharge chamber walls due to the flows of ions and electrons; Pxc — radiant flux from excited atoms to the walls; Pse is the electron flux on screen grid; Psi is the ion flux on the screen grid; Pxs is the radiant flux from excited atoms on the screen grid; Pxa is the radiant flux from excited atoms on the aceel grid; Pxout - radiant flux from excited atoms leaving through holes in the IOS; Pb is the power flux carried away with the beam ions (Figure 4).

The total heat flux to the discharge chamber walls can be written as the sum of the fluxes of each plasma component:

$$P_w = I_{we}(2T_e) + I_{wi}(0.5T_e + U_{iz} + \phi_w)\,, \qquad (19)$$

The flow of electrons slows down in the sheath layer by the floating potential ϕ_w, and comes to the wall with the energy that it had in the pre-sheath layer $-2T_e$. Ions with an energy of 0.5 T_e in the pre-sheath layer are accelerated by the potential ϕ_w. As a result of recombination, an energy equal to the ionization potential U_{iz} is released on the wall.

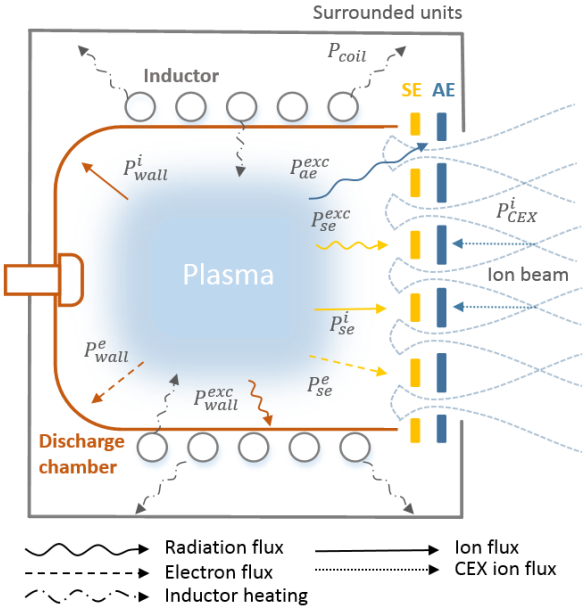

Figure 4. Distribution of heat fluxes from plasma to engine elements

The flow of electrons and ions to the screen electrode:

$$P_{se} = I_{se}(2T_e + w_s), \qquad (20)$$

$$P_{si} = I_{si}\left(\phi_s + \frac{1}{2}T_e + U_{iz} - w_s\right), \qquad (21)$$

where w_s is the electron work function from the screen grid material (for titanium 3.95 eV) expended during the recombination of an ion on a metal electrode.

In this model, it is assumed that all the energy spent on the excitation of neutral *Pex* atoms is given in the form of radiation to the surrounding surfaces.

Radiant flux from excited atoms to the walls of the discharge chamber and electrodes:

$$P_{xw} = \frac{A_w}{A}P_{ex}\,, \qquad (22)$$

$$P_{xs} = \frac{(1-f_s)A_s}{A}P_{ex}\,, \qquad (23)$$

$$P_{xa} = \frac{(1-f_s)f_aA_s}{A}P_{ex}\,, \qquad (24)$$

In the calculation, it was assumed that the optics are well focused and the beam ions practically do not touch the accelerating electrode. Consequently, the accelerating electrode is heated due to radiation from the plasma and the process of recharging neutral atoms in the ion beam, which creates a reverse current of slow ions on the accel grid. This process is the main factor determining the service lifetime of the ion-optical system. The current of charge exchange ions to the electrode is usually about 2% of the ion beam current.

The value of the ion flux is calculated from the equation:

$$P_{cex} = I_{cex}(U_a + U_{iz} - w_a)\,, \qquad (25)$$

where U_a is the potential on the accel grid, w_a is the work function of the electron from the accel grid material.

The power balance also contains flows leaving the engine that do not affect the temperature fields and the operation of the product.
The radiant flux of radiation from excited atoms leaving the thruster:

$$P_{xout} = \frac{f_s f_a A_s}{A} P_{ex}\,, \qquad (26)$$

And the fraction of power that goes with the ion beam:

$$P_b = I_b \left(\phi_s + \frac{1}{2} T_e + U_{iz}\right), \qquad (27)$$

E. Plasma distribution profile

In reality, the distribution of the plasma density of the RF discharge is not uniform in radius and length, and the change in parameters is determined by the following parameter:

$$h = \frac{n_i(r)}{n_i(0)}\,, \qquad (28)$$

Studies have shown that this parameter depends on the concentration of the neutral gas and the mean free path of the neutral-ion interaction:

$$\lambda_i = \frac{1}{n_g \sigma_i}\,, \qquad (29)$$

where σ_i is the total cross section of the neutral-ion elastic interaction.
Then, in the radial direction, the ion diffusion parameter [10, 13]:

$$h_r \approx \frac{0.8}{\sqrt{4 + \frac{R}{\lambda_i}}}\,, \qquad (30)$$

Based on the analytical [13] and experimental data, M. Dobkevicius and D. Feili [11] derived the dependence of the parameter change in the form:

$$h = \sqrt{1 - \left(\sqrt{1 - h_r^2}\,\frac{r}{R}\right)^2}\,, \qquad (31)$$

The obtained ion distribution profile was used to calculate the temperature fields in Chapter II.F.

F. Thermal and thermomechanical analysis

The initial data for calculating the temperature fields used were the heat losses of the conversion of the supplied electric power into traction, directly perceived by the construction of Chapters II.B and II.D.

In the thermal model, only two heat transfer mechanisms are used that correspond to vacuum conditions: radiant and thermal conductivity (including contact thermal conductivity, taking into account the actual areas of contact spots). In the radiant heat transfer model, the law of diffuse reflection and absorption is applied.

The results of the thermal calculation are the temperature fields in the thruster design (Figure 5), the temporal dynamics of their changes (time to reach a stationary solution) when the engine is turned on / off, its operation in mode, and when changing modes.

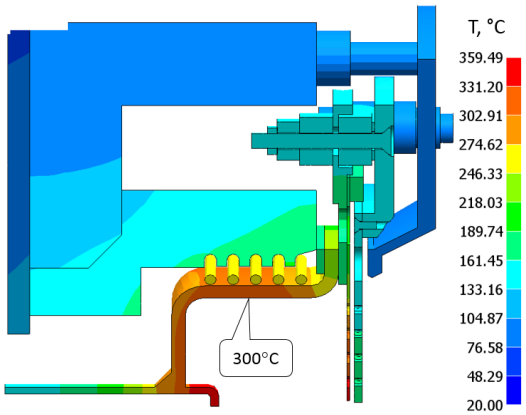

Figure 5. Stationary temperature field in the laboratory model of the engine with dissipated thermal power of 50 W, ° C

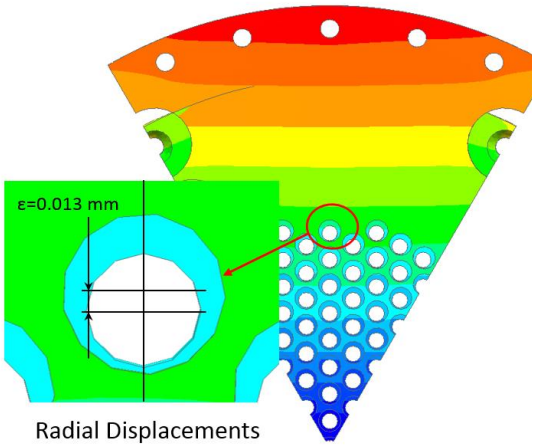

Figure 6. The result of modeling the thermal displacement of the electrodes

The data on temperature fields were then used in the iterative calculation cycle (Figure 1) to: clarify the boundary conditions on the walls of plasma-treated parts, clarify the temperature-dependent properties of models of structural materials (electromagnetic, thermal, mechanical) and to conduct thermomechanical analysis.

During the thermomechanical calculation of the engine design, the relative thermal displacements of the IOS electrodes (Figure 6) were determined (change in the electrode gap, decentration of the perforation holes), the relationship of these thermal displacements with the engine operating modes was revealed. The tasks were solved iteratively during the development of the engine by detailed modeling of the structure, taking into account the contact interaction of the parts and the conditions of their mates (tight fit, clearances, fastening torque). The thermomechanical strength was also evaluated to exclude possible damage (cracking of brittle ceramic parts, loosening of fasteners, etc.). Based on the simulation results, adjustments or changes to existing nodes were carried out.

III. Experimental setup

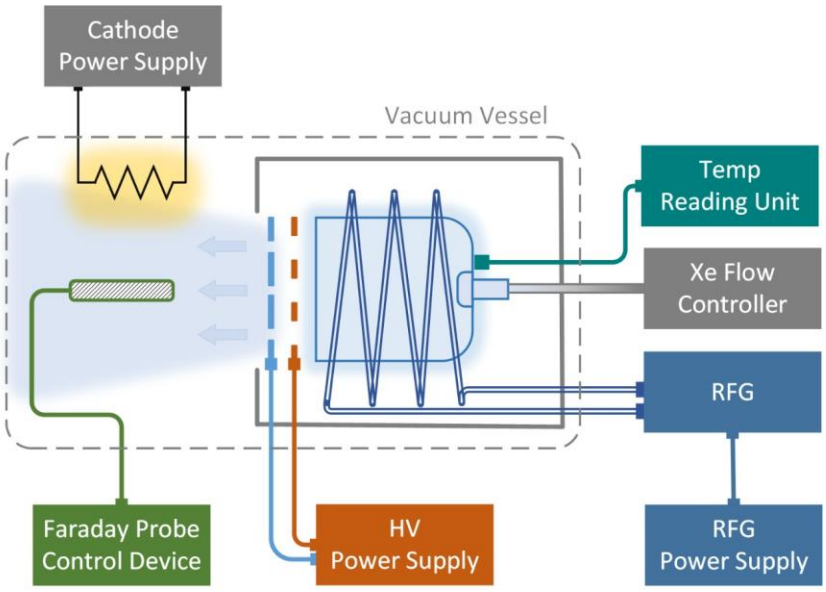

Figure 7. Experimental setup scheme

According to the proposed calculation schemes, a laboratory model of the RF ion thruster GT50 (Avant Space Systems LLC) was designed (Figure 7). The experimental results presented in Chapter IV correspond to a thruster assembly with a cylindrical quartz discharge chamber, a 5-turn antenna, and a two-electrode IOS, interelectrode gap was 0.8 mm.

Experimental studies of the engine were carried out on the basis of the Scientific Educational Center «Ion plasma technology» of Bauman Moscow State Technical University (Russia), in a vacuum chamber with a volume of 0.38 m3, vacuum pumping was carried out by a turbomolecular pump to a residual pressure of 1e-6 torr. Using a capacitive membrane MKS 627D, the pressure in the vacuum chamber was determined. Xenon mass flow was provided by the MKS GV50A flow regulator with an accuracy of setting 0.2% over the selected flow range. The maximum pressure at a flow rate of xenon 3 sccm was of the order of 7e-5 torr. The ion beam current was measured by the following methods: indirectly - as an electron current in the circuit of the screen electrode, and directly - using Faraday probes. Two types of probes were used in the experiment: the Faraday cup — a disk 18.2 cm in diameter and a side 78 mm high and a Faraday nude probe with a diameter of 8 mm.

The Faraday cup was used to determine the total beam current, located at a distance of 15 cm from the thruster exit section; the ion current was recorded using a Fluke 17B digital multimeter. The current in the emission electrode circuit was recorded using an internal high-voltage power supply measuring system developed by Avant Space Systems LLC, and was also duplicated using a Fluke 17B digital multimeter. Using the Faraday probe, the radial profile of the ion beam density was determined, measurements were taken at 6 points with a step of 1 cm, and the distance to the thruster exit section was 14 cm.

In order to study and verify temperature fields, at the bottom of the discharge chamber in the area of the injector, a platinum thermal resistance sensor was installed with automatic compensation in a three-wire circuit to eliminate the influence of heating of the input wires. All measured data using an automatic registration system recorded a file on a PC with a frequency of 1 Hz.

IV. Research results and analysis

Using the equipment described in Chapter III, a series of experiments was carried out to experimentally determine the characteristics of the ion beam and thruster operation modes (Figure 8).

The thruster studies were carried out using an RF generator developed by Avant Space Systems LLC [14], which ensures the operation of the engine at frequencies of 2-6 MHz at a power of up to 140 watts. The error in measuring the RF power is ± 5%, however, the error in setting the power mode is less than 0.1%. The engine was tested on xenon mass flow rate 1-3 sccm.

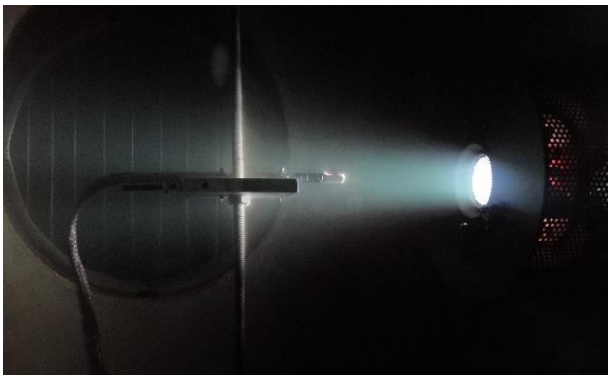

Figure 8. Thruster operation in a vacuum vessel using a Faraday probe

The main contribution to the error of ion current measuring using Faraday probes is associated with secondary emission processes from the collector surface. It is also necessary to take into account the error in determining the coefficient of secondary electron emission for xenon ions and the probe material, and as well as the error in the total area measuring of the collecting probe surface.

The most difficult to determine is the error introduced by resonant charge exchange, as a result of which part of the beam ions on the way to the probe become neutral atoms, which do not contribute to the total measured current [15]. Using these processes, we can estimate the relative error of the measurable current.

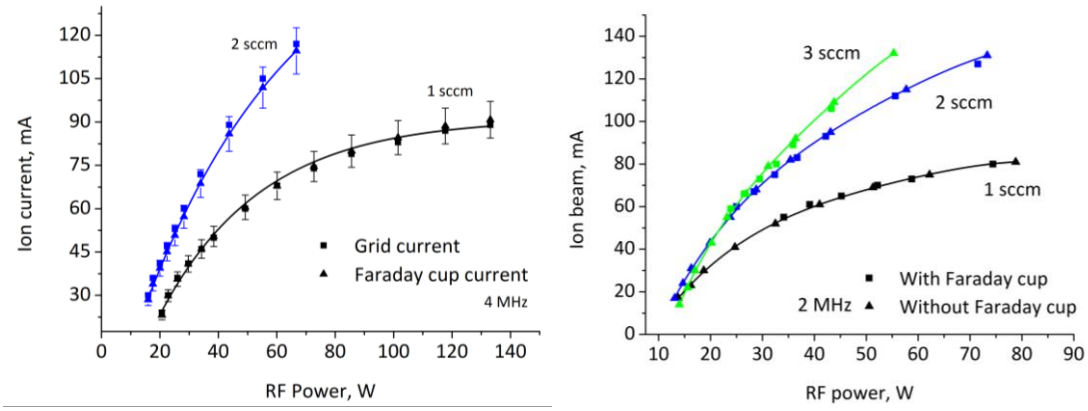

Рисунок 9. Comparison of measurements of the total beam current by the Faraday cup and current readings on the screen electrode

It was assumed that the presence of a Faraday cup in the path of the ion flux a will collect a neutral gas in itself and create a local increase in pressure. Thus, the Faraday cup would increase the reverse gas flows into the discharge chamber and change the thruster operating modes. However, comparing the readings of the current in the circuit of the screen grid with Faraday cup and without it (Figure 9), we can conclude that its presence has an insignificant effect on the engine operation mode.

The results of comparing the current recorded in the circuit of the screen electrode are presented and the current of the Faraday cup are presented in Fig. 9. Given the relative error in measuring the current of the Faraday Cup (for these conditions, about 12%) and the instrumental error in measuring the current in the electrode circuit is ± 1mA, the

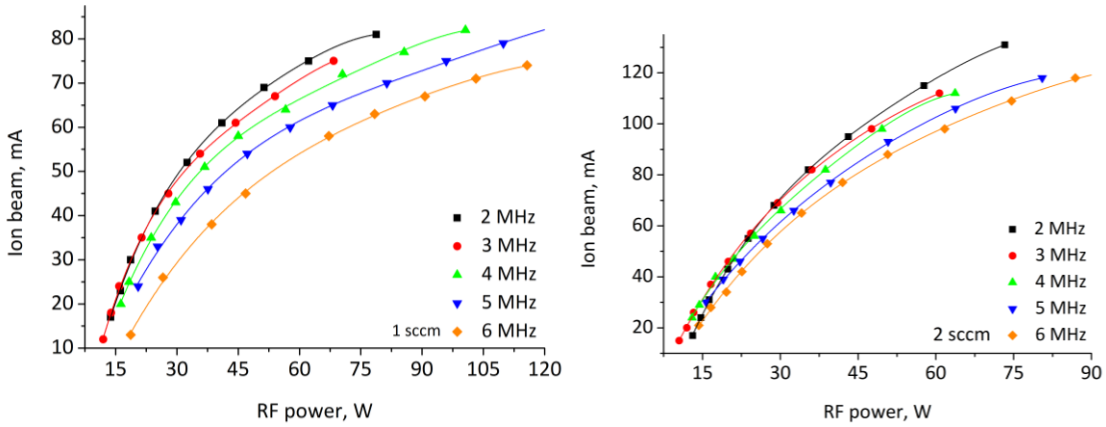

Figure 10. The measured values of the ion total current as a function of the RF generator frequency for operating modes 1 and 2 sccm

results give a good agreement. Consequently, we can conclude that it is legitimate to estimate the beam current from the current of the emission electrode and a small fraction of doubly ionized ions in a selected range of modes. In the future, it is planned to examine the last circumstance with using of a mesh energy analyzer.

The thruster parameters were compared at different frequencies (Figure 10). As the calculation of Chapter II.B showed, with increasing frequency, there is an increase in power losses as a result of heating of metal parts of the engine.

Therefore, there is a decrease in the discharge absorbed power. The validity of this conclusion is confirmed by experimental data, where, with increasing frequency, the ion beam current decreases at constant RF power.

Using the Faraday probe (Figure 11), the ion beam current density profile was determined for the mass flow rate of 1 and 2 sccm and the frequency of the RF generator 2 MHz. The Faraday probe under consideration was made of steel and did not have a guard ring, while the value of the collecting area of the probe exceeded the recommended value for the current density under study. The experiment was carried out without an ion beam neutralizer. In this regard, the measurements had a large error. As a result of this, when integrating the distribution of the ion current density, the total beam current turned out to be 2 times less than the current measured in the screen grid circuit. Therefore, Figure 11 shows only a qualitative picture of the distribution of the current density of the thruster beam.

During the study of the temperature fields of the engine, the temperature sensor was located on the outside of the discharge chamber. To exclude the influence of nonlinearities related to the heating processes of the structure on the recorded engine operation parameters, the engine was kept at one fixed input power for an hour (until the time of dependent readings of the temperature sensor reached a constant value). After that, the studied parameters of the engine were measured. The error of the temperature sensor was ± 2 ° C. Analysis of the experimental and calculated data gives an idea of the linear relationship between the temperature of the discharge chamber and the input power of the RF generator (Figure 12). Due to the uncertainty of the values of the blackness degree coefficient of the thrust materials and the surrounding vacuum chamber, as well as the not ideal contact surfaces of the parts, the calculated values of the temperature fields are overestimated. In this case, the functional dependence practically does not differ from the experimental one and the deviation between the values is approximately 80 °C.

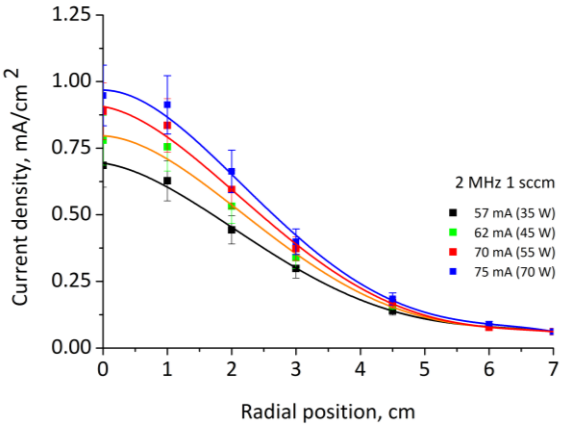

Figure 11. Ion current density profile measured using a Faraday probe

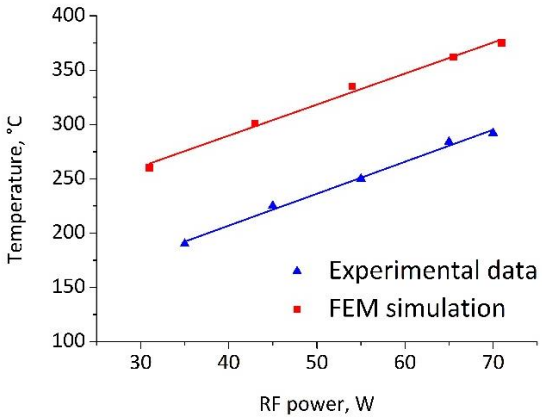

Figure 12. Comparison the discharge chamber temperature from simulation and experimental data for the 2 sccm and 2 MHz modes

The discrepancy between the calculated and experimental temperatures explains the need for further refinement of the thermal model of the engine in terms of boundary conditions. This will be realized by experimental refinement of the optical characteristics and contact thermal conductivities of structural elements, as well as subsequent verification of the model by the readings of thermal sensors located at several characteristic points of the thruster.

A complex calculation of the thruster was performed for the configuration and modes that corresponded to the above experiments. In the course of calculating the plasma parameters, an attempt was made to take into account the influence of the magnetic field of the inductor on the particle flow rate on the chamber walls as a result of ambipolar diffusion across the field. For this, according to the method proposed by D. Goebel [7], a coefficient was introduced for the particle flux, which was determined by the ratio of the ion velocity across the field and the Bohm velocity:

$$f_c = \frac{v_i}{v_{Bohm}}, \qquad (32)$$

Comparison of the calculation results for different series with a 2 MHz engine mode and 1 sccm mass flow rate are shown in Figure 13. The use of magnetic field corrections to a different extent reduces the deviation of the calculated and experimental data. In this case, the functional dependence of the beam current on the RF power changes greatly. The greatest coincidence with the experimental data has the option in which the confinement factor is 0.75. On the example of the calculated flow rate of 1.5 sccm, it can be seen that the theoretical curve fits well on the experimental points for the flow rate of 1 sccm, and for the experimental regime of 2 sccm a close simulation case for 3 sccm.

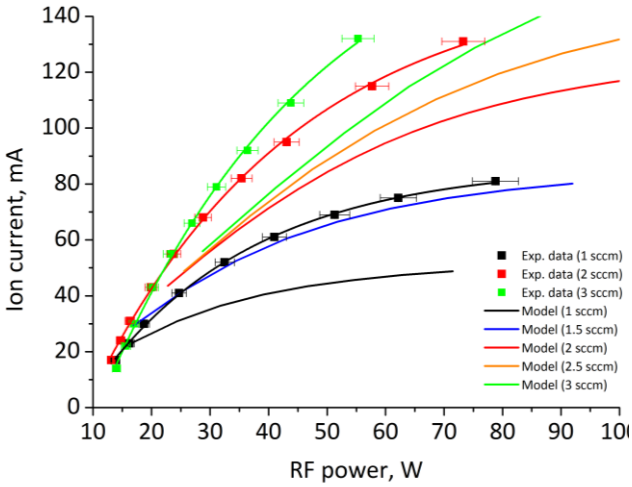

Figure 13. Comparison of simulation results and experimental data for the 2 MHz RF frequency

Such a deviation of the obtained data with good agreement of the functional dependence may be due to both inaccuracies in the calculation and in the experiment. Underestimated calculation results may be due to the low ionization efficiency compared to the experiment. Since the efficiency of ion formation depends on the xenon ionization cross section and the density of electrons and neutrals, it will increase with an increase in the density of neutrals. This determines the coincidence of the curves at different xenon mass flows. If the flow rate in the discharge chamber is specified exactly, then the error may be contained in determining the effective cross section for ionization of xenon atoms. For example, stepwise ionization or other phenomena that were not taken into account in this calculation can play a significant contribution.

On the other hand, the experiment was carried out in a relatively small chamber, the pressure of which at a flow rate of 1 sccm was 5E-5 torr. In this case, neutral flow back to the discharge chamber could have influenced the operating modes, thereby increasing the real flow rate and overestimating the real characteristics of the engine. In connection with these uncertainties, it is planned to study the effects of the degree of vacuum rarefaction on the engine characteristics, and expand the calculated plasma model taking into account the stepwise and double ionization of xenon atoms.

V. Conclusion

In the course of the research, a complex calculation approach for the RF ion engine was implemented taking into account losses due to induction heating and the mutual influence of the discharge plasma and the temperature fields of the thruster. Comparison of the calculated and experimental data gives good qualitative agreement. In this case, possible reasons for the quantitative discrepancy with the experiment were identified, such as the need to take into account stepwise and double ionization in the plasma model, and the refinement of material characteristics for the thermal model. On the other hand, ways were proposed to refine the obtained experimental data. In general, the complex scheme has proved its worth in the design of radio-frequency ion thruster of the classical scheme.

In the future, a large amount of work is planned on the study of RF ion thruster. The calculation scheme based on the fluid plasma model will be refined taking into account stepwise ionization and the influence of the magnetic field. In parallel with this, a kinetic plasma model is being developed to describe the discharge in the presence of an external magnetic field. In the future, this model will be integrated into the current simulation cycle. In order to verify the models, a number of experimental studies of the RF discharge in a magnetic field are planned. Measurements will include the use of Faraday probes to measure the integral parameters of the beam, as well as a three-electrode Langmuir probe to distribute local plasma parameters in the gas discharge chamber of the engine.

Acknowledgments

We would like to express our thanks to members of the Scientific-Educational Centre «Ion-plasma technologies» at Bauman Moscow State Technical University (Russia) for their help in assisting in experimenting and providing laboratory resources, their fruitful discussions and comments. This work was supported by Skolkovo Foundation, Russian Federation Grant Number G11/19.

References

[1] Grush L., “SpaceX just launched two of its space internet satellites — the first of nearly 12,000”, [online journal], 2018, URL https://www.theverge.com/2018/2/15/17016208/spacex-falcon-9-launch-starlink - MICROSAT-2a-2b-Paz-clock-live [cited 11 September 2019].

[2] Oneweb official website. URL https: //www.oneweb.world/ [cited 10 September 2019].

[3] Olenson S.R, Sankovic J.M. “Electric propulsion for low Earth orbit constellation”, NASA/TM-1998-208821. URL http://ntrs.nasa.gov/archive/nasa/casi.ntrs.nasa.gov/19990008485.pdf [cited 7 September 2019].

[4]Aleksandrov A.F., Bugrov G.E., Kerimova I.F., Kondranin S.G., Kralkina E.A., Pavlov V.B., Plaksin V.Y., Rukhadze A.A., Vavilin K.V. “Self-consistent model of an RF inductive plasma source located in an external magnetic field”, Journal of Russian Laser Research, Vol. 24, 2003, pp. 301-321.

[5] Kalvas, T., Tarvainen, O., Ropponen, T., and et al. (2010). IBSIMU: a three-dimensional simulation software for charged particle optics. Review of Scienti_c Instruments, 81(2):02B703.

[6] P. Chabert, J. Arancibia Monreal, J. Bredin, L. Popelier, and A. Aanesland, “Global model of a gridded-ion thruster powered by a radiofrequency inductive coil” // Physics of Plasmas 19, 073512. 2012.

[7] D. M. Goebel, “Analytical Discharge Model for RF Ion Thrusters” // IEEE Trans. Plasma Sci. 36, 2111 (2008).

[8] D. Goebel and I. Katz, Fundamentals of Electric Propulsion: Ion and Hall Thrusters, 1st ed. (Wiley, 2008).

[9] F. F. Chen. Introduction to Plasma Physics and Controlled Fusion, volume 1. Plenum Press, New York, N.Y., second edition edition, 1984

[10] Chabert, P. and Braithwaite, N. (2011). Physics of Radio-Frequency Plasmas. Cambridge University Press, Cambridge.

[11] Dobkevicius M., Feili D. A coupled performance and thermal model for radio-frequency gridded ion thrusters //The European Physical Journal D. – 2016. – Т. 70. – №. 11. – С. 227.

[12] Van Noord, J. L. NEXT Ion Thruster Thermal Model. National Aeronautics and Space Administration, Glenn Research Center, 2010

[13] A. Lieberman, M. Lichtenberg, Principles of Plasma Discharges and Materials Processing, 2nd edn. (John Wiley & Sons, New Jersey, 2005)

[14] Surminskii A.A., Ayupov R.E. “Development of compact high efficiency RF generator for inductive coupled plasma sources”, IEPC Paper No. 2019-464. Proceedings of the 36rd International ElectricPropulsion Conference, Vienna, Austria 2019.

[15] Daniel L. Brown. Recommended Practice for Use of Faraday Probes in Electric Propulsion Testing // Journal of Propulsion and Power 33(3), September 2016